High-power electrostatic free-electron maser as a future source for fusion plasma heating: Experiments in the short-pulse regime

W. H. Urbanus,* W. A. Bongers, C. A. J. van der Geer, P. Manintveld, J. Plomp, J. Pluygers, A. J. Poelman, P. H. M. Smeets, and A. G. A. Verhoeven
FOM Instituut voor Plasmafysica Rijnhuizen, Association EURATOM-FOM, Postbus 1207, 3430 BE Nieuwegein, The Netherlands

V. L. Bratman, G. G. Denisov, A. V. Savilov, and M. Yu. Shmelyov
Institute for Applied Physics, 46 Uljanova Street, Nizhny Novgorod 603600, Russia

M. Caplan
Lawrence Livermore National Laboratories, P.O. Box 808, Livermore, California 94551

A. A. Varfolomeev, S. V. Tolmachev, and S. N. Ivanchenkov
Russian Research Centre ''Kurchatov Institute,'' Moscow 123182, Russia
(Received 9 November 1998)

A high-power, frequency-tunable electrostatic free-electron maser, being developed at the FOM Institute for Plasma Physics ''Rijnhuizen,'' shows lasing at various frequencies. An output power of 730 kW at 206 GHz is generated by a 7.2-A, 1.77-MeV electron beam, and 380 kW at 165 GHz is generated by a 7.4-A, 1.65-MeV electron beam. In the present experimental setup, without recovery of the spent electron beam power, the pulse length is limited to 12 μs. Nevertheless, the main issues, such as the possibility of high-power, single-mode operation and frequency tuning, have been confirmed. The experimental results and the dynamics of the laser process are well in accordance with simulations. [S1063-651X(99)03905-7]

PACS number(s): 41.75.Ht, 29.17.+w

I. INTRODUCTION

The principle aim of present free-electron maser (FEM) research is the realization of a source of mm-wave radiation of high average power, high system efficiency, and frequency tunability over a large range [1]. The achievement of these targets may culminate in the use of FEMs as power sources for electron-cyclotron applications on magnetically confined plasmas in future fusion research devices, such as the International Thermonuclear Experimental Reactor. For such applications power units of at least 1 MW of mm-wave power in the frequency range from 140 to 200 GHz at a system efficiency of 50% are required. Fast tunability (on the ms scale) in a frequency range of a few percent would be a major advantage.

In an FEM, i.e., a free electron laser (FEL) operating in the mm-wave regime, radiation is generated by a relativistic electron beam oscillating in an undulator. The radiation wavelength is determined by the electron beam energy (Doppler shift) and the period and field strength of the undulator. A promising approach to realize both fast frequency tuning via the electron beam energy and a high system efficiency involves the use of electrostatic electron beam acceleration and deceleration with electron beam energy recovery [1–4]. In this scheme the electron beam is accelerated to the interaction region, i.e., the undulator and the cavity, and afterwards it is decelerated and collected in a multistage depressed collector. On deceleration, the electron beam transfers most of its energy back to the accelerator voltage supply, thus limiting the required power. The high voltage power supply has to deliver only the beam loss current.

The electronic efficiency, i.e., the fraction of the electron beam power, which is transferred to mm-wave power, is of the order of 5%. This is considerably lower than in gyrotrons [5]. In the FEM a low electronic efficiency has been chosen as a trade-off between required electron beam power on the one hand and ease of beam recovery on the other hand. A high electronic efficiency causes a too high energy spread after the FEL interaction, complicating both beam transport through the energy recovery section and the process of recovery itself, while a lower electronic efficiency requires a higher electron beam current. Nevertheless, when the energy recovery system is installed, the system efficiency, i.e., the efficiency from mains power to mm-wave output power, will be much higher. After deceleration the electrons will be collected at an average energy of 60 keV [6]. At 12-A beam current the dissipated power in the collector will be some 720 kW. Additionally, some 200 kW will be dissipated in the high voltage system and auxiliary equipment. Thus, in spite of the rather low electronic efficiency, the system efficiency will exceed 50%. This is slightly higher than the system efficiency of state of the art gyrotrons [5].

The mm-wave power is generated in an oversized corrugated waveguide, mounted inside a step-tapered undulator [6,7]. In the following we call this the operating waveguide. The feedback system of the cavity is formed by two newly developed reflectors, which are segments of a stepped waveguide [8]. In these reflectors, two off-axis beams are formed after some distance via multiplication of the quasioptical beam emerging from the operating waveguide. The off-axis beams are reflected by flat copper mirrors and merge back

*FAX: +31-30-6031204. Electronic address: urbanus@rijnh.nl

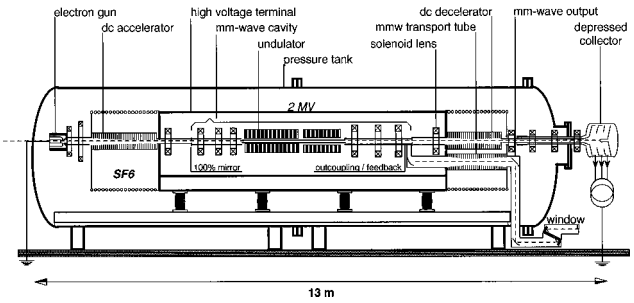

FIG. 1. Layout of the FEM. In the experiments described here the decelerator tube and the depressed collector were not installed. The device is mounted in a SF_6-filled pressure tank for voltage hold off. The mm-wave transport tube serves to transport the mm-wave beam in a vacuum from the high-voltage terminal to earth potential.

into one beam, which enters the operating waveguide.

In this paper we present experimental results on generation of high-power mm-wave radiation in the FEM being developed at the FOM Institute for Plasma Physics ''Rijnhuizen,'' The Netherlands [9]. Results are presented on lasing around 200 GHz and 165 GHz. Since no electron beam energy recovery system is installed yet, the pulse length is limited to 12 μs. A net output power of 730 kW is reached for a 7.2-A, 1.77-MeV electron beam. It is demonstrated that the FEM can operate in single-frequency mode. The output beam has a Gaussian mode content exceeding 99.8%, both for 200 GHz and 165 GHz.

II. EXPERIMENTAL SETUP

The layout of the Fusion FEM is shown in Fig. 1. The setup is largely determined by the requirement for low-loss electron beam transport and the capability to handle high-power mm-wave radiation during long pulses. To ensure low-loss electron beam transport, and to make frequency tuning via the electron beam energy straightforward, a straight beam line with solenoid focusing is used [10].

The mm-wave cavity consists of a waveguide inside the undulator and so-called stepped waveguides upstream and downstream of the undulator, see Fig. 2 [8]. This arrangement forms a low-Q cavity as typically 50 to 70% of the power generated is coupled out. A rectangular corrugated waveguide is used, which carries a hybrid HE_{11} mode. This mode is strongly peaked in the center, which results in strong interaction with the electron beam and ensures low Ohmic losses as well. The waveguide is 1.5 m long and has a cross section of $15\times 20\ \mathrm{mm}^2$. The vertical sides (parallel to the undulator magnetic field) are corrugated. Ohmic losses are further reduced by operating the FEM with a low feedback coefficient of the mm-wave cavity, which decreases the total intracavity power.

The straight electron beam line eliminates the use of on-axis mirrors. In the stepped waveguides the operating HE_{11} beam is split into two identical off-axis beams. Full separation of the beams takes place at a distance $D_{\mathrm{sep}}=a^2/2\lambda$, with a the height of the stepped waveguide and λ the radiation wavelength. Two off-axis mirrors, with an opening in between to let the electron beam pass through, reflect the beams. The backward propagating beams merge back into one beam. This way, a 100% reflector is realized at the upstream side of the undulator. At the downstream side a similar system is used, but here one of the mirrors can be shifted in a longitudinal direction (direction of beam propagation). Upon propagating backwards, the beams have a phase difference, which results into one on-axis beam and two off-axis beams. The on-axis beam constitutes the feedback power, the two off-axis beams are coupled out. By adjusting the position of one single mirror, the feedback can be varied between 0 and 100%.

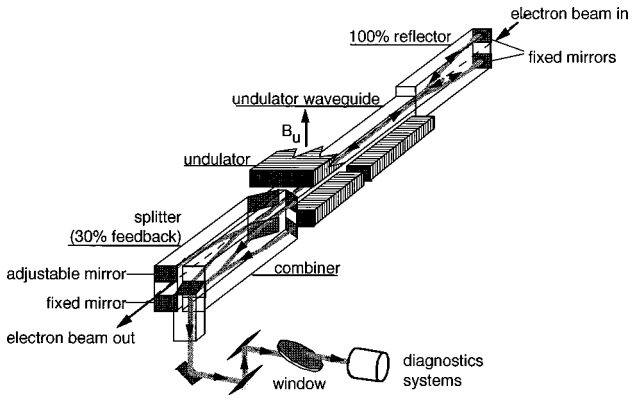

FIG. 2. Layout of the mm-wave cavity, showing the upstream reflector waveguide, the operating waveguide inside the undulator, and the downstream reflector waveguide. Parallel to the latter a waveguide is mounted, in which the two beams coupled out from the downstream reflector are recombined into one output beam. Schematically, the boron-nitride window and the mm-wave diagnostics are given.

The two off-axis beams are recombined back into one beam in another stepped waveguide, parallel to the outcoupling waveguide. Finally, a Brewster-angle boron-nitride window is used as a vacuum barrier. A Brewster-angle window is chosen to provide full transmission over a wide frequency band.

Low power testing of the cavity shows that the feedback bandwidth is about 4%, see Fig. 3 [11]. Around 200 GHz losses are of the order of a few per cent but increase considerably at other frequencies, e.g., at 170-GHz losses are of the order of 25% single pass. The high losses are due to mechanical imperfections of the operating waveguide. This waveguide will be improved.

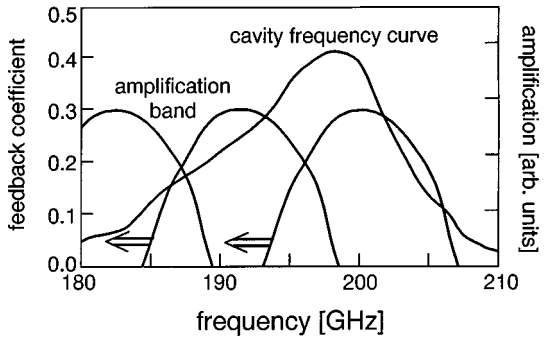

FIG. 3. Feedback frequency response of the cavity, when tuned to a central frequency of 200 GHz and a feedback coefficient of 0.50. As an example, amplification curves are given schematically for three different positions of the amplification band, i.e., three settings of the electron beam energy.

At high-power level the interaction between the electron beam and the mm-wave beam is further improved by a step-tapered undulator [7,12]. The first 20 periods have a strength of 0.20 T and the latter 16 periods have a strength of 0.16 T. The period length is 40 mm. At the entrance of the first section, electrons are in synchronism with the mm wave. Upon interaction the electrons lose energy and, consequently, go out of synchronism. Due to the lower undulator field in the second section, the electrons obtain additional longitudinal velocity, and synchronism is restored. Between the two undulator sections is an adjustable field-free region, which determines the phase of the electron bunches with respect to the radiation wave at the entrance of the second section. According to simulations, the electronic efficiency is about 5% [12].

III. SIMULATIONS ON MODE COMPETITION

An important issue in oscillators is the possible excitation of transverse and longitudinal parasitic modes. This depends on the transverse dimensions of the operating waveguide where it concerns transverse modes. The operating waveguide measures $15\times 20\ \mathrm{mm}^2$, which is needed for proper electron beam transport. Consequently, the waveguide is many times overmoded. The reflectors are strongly mode selective and provide weak feedback for modes other than the HE_{11} mode. Consequently, parasitic modes are not properly fed back and will not grow to high power levels. Further, nonlinear suppression of parasitic transverse modes is enhanced too by the mode-selective character of the operating waveguide [13]. In addition, excitation of parasitic transverse modes is not resonant and, therefore, takes place only by their coupling through the electron beam with the operating HE_{11} mode.

With respect to parasitic longitudinal modes, i.e., modes with the same transverse structure but with different frequencies, the frequency dependency of the feedback system and the parameter of excess over threshold of single-mode operation L are important. In the simplest model, the parameter L is defined as the product of the length of the operating region and the cubic root of the electron beam current. If L exceeds its starting value and is less than some threshold, the single-mode operation is stable. When L exceeds the threshold of single-mode operation, complicated multimode operation can take place [14,19].

For the fusion FEM, a long interaction region and a relatively high electron beam current result in a rather large value of L. In addition, the step-tapered undulator and the rather broadband feedback system complicate the dynamics of the oscillator. In order to simulate this process, a nonstationary, spatiotemporal approach has been used [14,18,19]. A 1D code based on this approach was improved by taking into account the motion of the wave inside the frequency-dispersive reflectors [16], as well as ac space charge effects and undulator tapering. Results of this code have been confirmed by other codes based on the mode-temporal approach [13,15,17]. Simulation results show that, in spite of the fact that the parameter L is quite large for the operating parameters of the fusion FEM, the output beam contains only a small longitudinal parasitic-mode content.

At constant electron beam energy, the process of power buildup roughly follows four stages [15]. In stage I a number of modes grow from noise. Since the power level is low, there is no interaction between the modes and no suppression of modes by one main mode. When the feedback of the cavity is independent of frequency, all modes grow roughly at a rate corresponding to the profile of the amplification band. When the feedback depends on frequency, both the profile of the amplification band and the feedback influence the growth rate of the various modes.

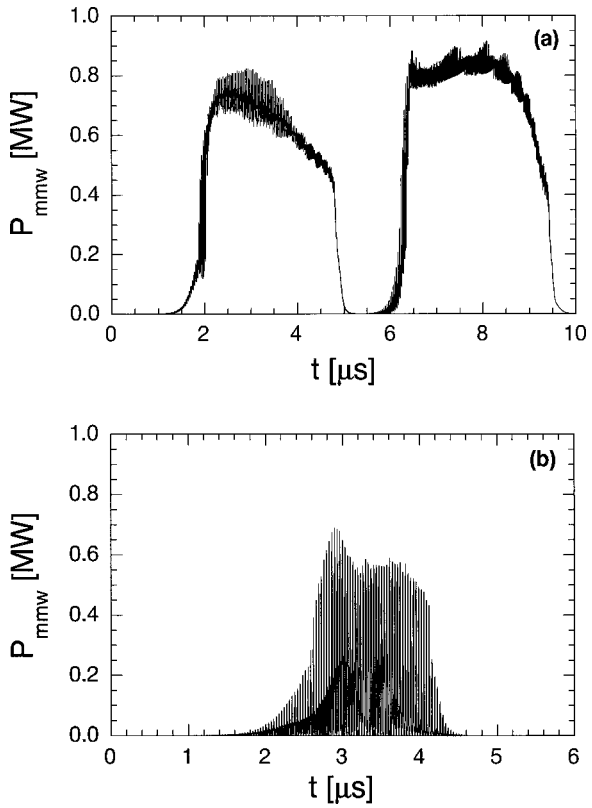

FIG. 4. Simulation results on the mm-wave output power P_{mmw} for the situation of high (a) and low (b) initial electron beam energy.

In stage II of the process, the fast growing modes (with frequencies close to the center of the amplification band) grow to the nonlinear regime. At the beginning of this stage these fast-growing modes suppress modes with a lower growth rate, i.e., modes farther away in frequency. Then, one of the fast-growing modes suppresses all other modes. Evidently, the process of mode suppression will be stronger and faster when the product of amplification and feedback is a function of frequency.

In stage III, due to the increase of the power of the single mode, new parasitic modes rather far from the center of the amplification band, and having been suppressed in stage II, can be excited so that the output signal fluctuates strongly and fast as a function of time. However, when the feedback is small for the parasitic modes, which have other frequencies than the main mode, they cannot grow to a significant power level and die out. In that case, again the oscillator operates in single-mode regime (stage IV).

In the experiment, the two major effects determining the power buildup are the feedback, which is frequency dependent, and the rate of the electron beam energy drops, which shifts the amplification band in time and thus determines the

interaction time for a specific mode. Consequently, the process of power buildup is strongly dependent on the position of the amplification band, i.e., the electron beam energy, with respect to the feedback curve. Basically, there are two major differences between the cases of proper initial beam energy and low initial beam energy. For the case of proper initial beam energy both the product of feedback times amplification and the interaction time are sufficient to reach the stage where mode competition takes place and one main mode suppresses all other modes. In this case stages III and IV of the interaction process are passed, see Fig. 3 and Fig. 4(a).

When the initial beam energy is low, mm-wave power is generated at relatively low frequencies for which the feedback is low. Further, the amplification band runs out of the cavity curve in a short time. The buildup of power does not reach the nonlinear regime and, consequently, no mode competition takes place. The spectrum shows several frequencies and the power fluctuates strongly, see Fig. 4(b).

The simulations show that once the power starts up at a specific frequency, it remains at that frequency even though the amplification band shifts with dropping electron beam energy. The mm-wave power dies out when the amplification band shifts too far away. Then the power starts up again, at a lower frequency. Obviously, the frequency steps are of the order of the width of the amplification band, which is of the order of 5 GHz.

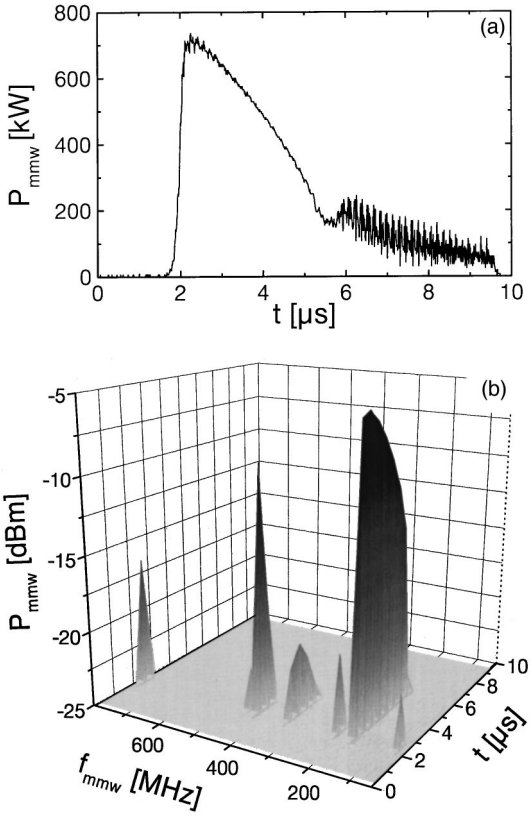

FIG. 5. Highest output power P_{mmw} achieved so far, reaching just over 730 kW (a). The electron beam current and beam energy at the start of the pulse are 7.2 A and 1.772 MeV, respectively. The feedback coefficient is 0.55. The spectrum, shifted down in a heterodyne mixer, shows a number of frequencies at startup, but after a few μs one mode suppresses all others and remains stable until the end of the pulse (b).

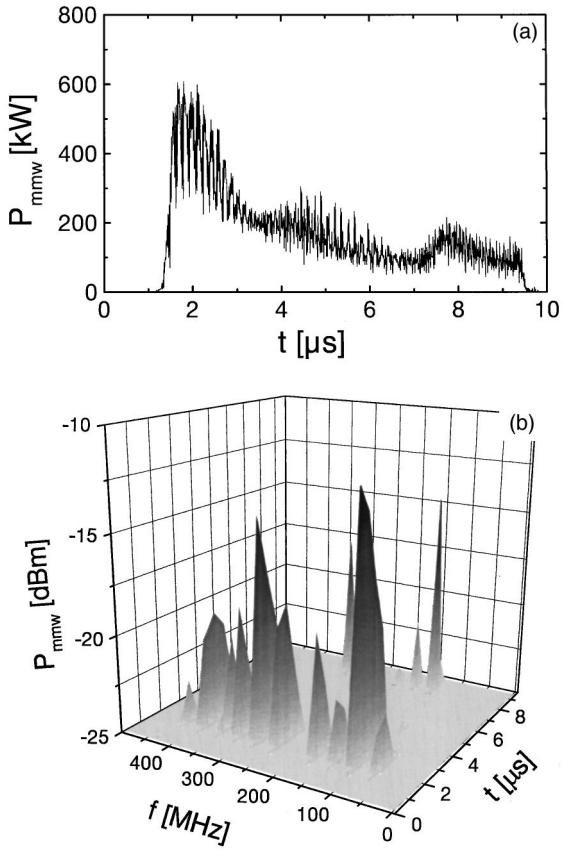

FIG. 6. Output power P_{mmw} generated by a 7.2-A, 1.76-MeV electron beam (a). The feedback coefficient is 0.55. The frequency spectrum shows that two longitudinal modes are present (b).

IV. EXPERIMENTAL RESULTS

In the present setup (without energy beam recovery), the accelerating voltage drops rapidly during the pulse (1 kV per ampere of beam current per μs). The bandwidth of the cavity is some 4% and, consequently, the amplification band rapidly shifts across the cavity bandwidth. Thus, the pulse length is limited to a few μs and the output power is not constant during the pulse. Experiments on generating mm-wave output power have been done for two settings of the electron beam energy, i.e., for two frequencies. For each setting, parameters such as feedback of the cavity, drift gap between the two undulator sections, and the electron beam energy, have been varied. The electron beam current is constant during the pulse.

For optimized feedback (0.55), 730 kW of power was generated for a 7.2-A electron beam (see Fig. 5). The electron beam energy at the start of the pulse is 1.772 MeV, and drops with 7.2 keV/μs. At this beam energy single-mode operation is reached, as shown in the frequency spectrum (given on a logarithmic scale). At startup several frequencies are excited, but after a few μs the main frequency suppresses the parasitic frequencies. It is clearly seen that, in spite of the drop of the electron beam energy, the frequency locks to a specific value. For a slightly lower electron beam energy at start of 1.76 MeV, a multifrequency output beam is gener-

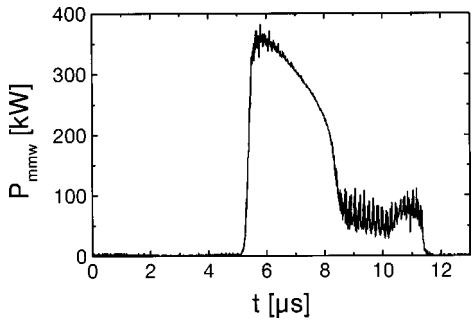

FIG. 7. Output power around 160 GHz, P_{mmw}, for a 1.61-MeV, 7.1-A electron beam. The pulse first shows single-frequency operation, followed by multifrequency operation for the then lower electron beam energy.

ated, see Fig. 6. The spectrum shows a number of frequencies at start. Contrary to the situation given in Fig. 5, during the pulse, two modes keep oscillating, thus resulting in strongly fluctuating output power.

Tunability of the FEM was demonstrated by operation around 165 GHz. Around this frequency power losses in the cavity are much higher, close to 25% single pass, and thus the output power is significantly lower. However, in spite of these high losses, for a sufficiently high product of feedback times amplification single-frequency output is possible, as is shown in Fig. 7. For a 7.4-A, 1.603-MeV electron beam, first single-frequency output is generated, followed by fluctuating multifrequency output when the electron beam energy has dropped. Note that in principle single-frequency operation can be reached for every frequency, by adjusting the cavity, i.e., the feedback curve, such that the peak of the feedback curve coincides with the peak of the amplification band.

For most applications it is important that the output beam has a Gaussian profile. In many cases the radiation source and the application, e.g., a tokamak reactor, will be a considerable distance apart. For loss-free beam transport, a Gaussian output beam is essential. The spatial power distribution has been measured with a heat-absorbing foil and an infrared camera. Typical results are shown in Fig. 8, for a 206-GHz beam and a 167-GHz beam. In both cases the Gaussian mode content exceeds 99.8%.

V. CONCLUSIONS

The fusion FEM generates 730 kW of mm-wave power at 200 GHz, for a 7.2-A 1.77-MeV electron beam. For this frequency the electronic efficiency is 5.7%, which is slightly higher than expected. These results were obtained with low

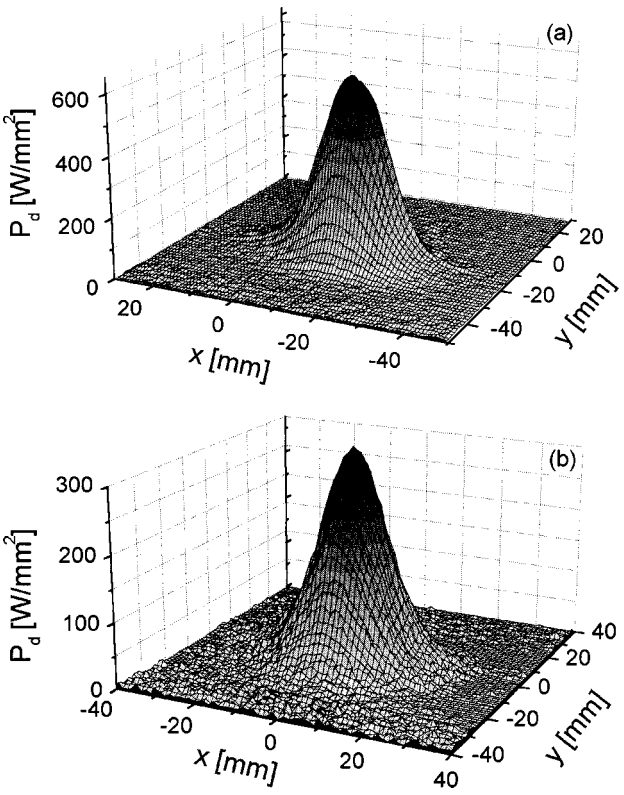

FIG. 8. Spatial power density P_d profiles for a 206-GHz beam (a) and a 167-GHz beam (b), as measured with a heat-absorbing foil and an infrared camera.

cavity losses. For another setting, with higher cavity losses, the output power is lower. Around 160 GHz, 380 kW of output power is generated by a 7.2-A electron beam. Although the cavity losses are frequency dependent, for all cases, the process of power buildup and mode competition is in principle similar; depending on the electron beam energy at the start of the pulse, either a high-power, single-frequency output beam is generated, or a strongly fluctuating multifrequency beam is generated. The start-up time and in particular the relation between the frequency spectrum of the mm-wave beam and the electron beam energy are predicted well by simulations.

ACKNOWLEDGMENTS

This work was performed as part of the research program of the association agreement of EURATOM and the Stichting voor Fundamenteel Onderzoek der Materie (FOM) with financial support from the Nederlandse Organisatie voor Wetenschappelijk Onderzoek (NWO) and EURATOM.

[1] W. H. Urbanus, W. A. Bongers, G. van Dijk, C. A. J. van der Geer, J. P. van Ieperen, A. van der Linden, P. Manintveld, A. B. Sterk, A. V. Tulupov, A. G. A. Verhoeven, M. J. van der Wiel, V. L. Bratman, G. G. Denisov, A. A. Varfolomoeev, S. N. Ivanchenkov, A. S. Khlebnikov, M. Catellino, A. Salop, and M. Caplan, Nucl. Instrum. Methods Phys. Res. A **358**, 155 (1995).

[2] L. R. Elias, G. Ramian, R. J. Hu, and A. Amir, Phys. Rev. Lett. **57**, 424 (1986).

[3] G. Ramian, Nucl. Instrum. Methods Phys. Res. A **318**, 225 (1992).

[4] A. Abramovich, A. Arensburg, D. Chairman, A. Eichenbaum, M. Dranzin, A. Gover, H. Kleinman, I. Mershasin, Y. Pinhazi, J. S. Sokolowski, Y. M. Yakover, M. Cohen, L. A. Levin, O.

Shahal, A. Rosenberg, J. Schnitzer, and J. Shiloh, Appl. Phys. Lett. **71** (26), 3776 (1997).

[5] K. Felch, H. R. Jory, J. A. Lorbeck, C. M. Loring, Y. M. Mizuhara, J. M. Neilson, R. Schumacher, and R. J. Temkin, IEEE Trans. Plasma Sci. **24**, 558 (1996).

[6] C. A. J. van der Geer, M. Caplan, N. Dione, S. B. van der Geer, M. J. de Loos, A. G. A. Verhoeven, M. Valentini, M. J. van der Wiel, and W. H. Urbanus, Nucl. Instrum. Methods Phys. Res. A **407**, 70 (1998).

[7] A. A. Varfolomeev and A. H. Hairetdinov, Nucl. Instrum. Methods Phys. Res. A **341**, 462 (1994).

[8] G. G. Denisov and M. Yu. Shmelyov, in Proceedings of the 21st International Conference on IR & MM Waves, edited by M. von Ortenberg and H. U. Müller [Conf. Proc. Berlin **1**, BF3 (1996)].

[9] W. H. Urbanus, W. A. Bongers, G. van Dijk, C. A. J. van der Geer, R. de Kruif, P. Manintveld, J. Pluygers, A. J. Poelman, F. C. Schüller, P. H. M. Smeets, A. B. Sterk, A. G. A. Verhoeven, M. Valentini, and M. J. van der Wiel, Nucl. Instrum. Methods Phys. Res. A **407**, 327 (1998).

[10] M. Valentini, C. A. J. van der Geer, A. G. A. Verhoeven, M. J. van der Wiel, and W. H. Urbanus, Nucl. Instrum. Methods Phys. Res. A **390**, 409 (1997).

[11] W. A. Bongers, P. Manintveld, G. van Dijk, B. S. Q. Elzendoorn, C. A. J. van der Geer, R. de Kruif, J. Pluygers, A. J. Poelman, P. R. Prins, F. C. Schüller, M. Valentini, A. G. A. Verhoeven, M. J. van der Wiel, and W. H. Urbanus, in *Proceedings of the 10th Workshop on ECE and ECRH, EO10*, edited by A. J. H. Donné and A. G. A. Verhoeven (World Scientific, Singapore, 1998), p. 507.

[12] M. Caplan, R. W. B. Best, A. G. A. Verhoeven, M. J. van der Wiel, W. H. Urbanus, V. L. Bratman, and G. G. Denisov, Nucl. Instrum. Methods Phys. Res. A **331**, 243 (1993).

[13] V. L. Bratman, G. G. Denisov, A. V. Savilov, M. Yu. Shmelyov, A. G. A. Verhoeven, and W. H. Urbanus, Nucl. Instrum. Methods Phys. Res. A **407**, 40 (1998).

[14] N. S. Ginzburg and A. S. Sergeev, Zh. Tekh. Fiz. **61**, 133 (1991) [Sov. Phys. Tech. Phys. **36**, 79 (1991)].

[15] V. L. Bratman and A. V. Savilov, Nucl. Instrum. Methods Phys. Res. A **358**, 182 (1995).

[16] A. V. Savilov, Opt. Commun. **123**, 133 (1996).

[17] M. Caplan, B. Levush, T. M. Antonsen, Jr., A. V. Tulupov, and W. H. Urbanus, Nucl. Instrum. Methods Phys. Res. A **358**, 174 (1995).

[18] T. M. Antonson Jr. and B. Levush, Phys. Fluids B **1**, 1097 (1989).

[19] Ya. L. Bogomolov, V. L. Bratman, N. S. Ginzburg, M. I. Petelin, and A. D. Yamakowsky, Opt. Commun. **36**, 209 (1981).